Badar, Tabish; Backman, Juha; Visala, Arto

Modeling of Tire Lateral Forces in Non-linear 6-DOF Simulations for Off-Road Vehicles

Published in:
IFAC-PapersOnLine

DOI:
10.1016/j.ifacol.2022.11.107

Published: 15/09/2022

Document Version
Publisher's PDF, also known as Version of record

Available online at www.sciencedirect.com

ScienceDirect

IFAC PapersOnLine 55-32 (2022) 12–17

Modeling of Tire Lateral Forces in Non-linear 6-DOF Simulations for Off-Road Vehicles ⋆

Tabish Badar * Juha Backman *,** Arto Visala *

* Department of Electrical Engineering and Automation, Aalto University, 02150 Espoo, Finland (e-mails: firstname.surname@aalto.fi)
** Farming technologies, Natural Resources Institute Finland (Luke), Lönnrotinkatu 7, 50100 Mikkeli, Finland (e-mail: juha.backman@luke.fi)

Abstract: This study highlights the use of a linear model to generate lateral forces in a nonlinear vehicle driving simulation. The crucial thing about modeling lateral forces is the centripetal acceleration limit a ground vehicle may experience. One can employ a linear model to simulate lateral forces when the commanded lateral acceleration for an off-road car-like vehicle (such as Polaris – an electric all-terrain vehicle) is limited to 3 m/s^2, and for a heavy forest truck (for example, Ponsse's Bison – a forwarder) to about 1 m/s^2. Tire construction, which plays a significant role in the load-carrying capability and the cornering of a ground vehicle, is considered in this paper. An estimate of the cornering stiffness for the tires is determined using Hewson's model, which uses only the basic information mentioned in their datasheets. At the maximum rated load, a cornering stiffness coefficient value is obtained. The cornering coefficient is used to simulate lateral forces as the function of vertical load and sideslip angle. The simulation results highlight the advantages and deficiencies of using a linear tire model to generate lateral forces for off-road vehicles. Finally, the simulation data is analyzed, where the results are compared with those obtained from a standard kinematic model.

Keywords: Tires, Cornering Stiffness, Vehicle Handling, Vehicle Modeling and Simulation.

1. INTRODUCTION

Forests are the most important natural resource in harvesting. In Finland, forests cover over 70% of the land with annual growth of around 107 million cubic meters, and the total is 94 million cubic meters. At Aalto University, one of the research and development platforms for autonomous driving in uneven terrains is Polaris electric All-terrain vehicle (e-ATV). ATVs are used by farmers and loggers in forests. The other machine of interest is Ponsse's Bison forwarder, which serves the purpose of transporting cut-to-length logs from forest stands to roadside. The main aspect of this study involves the demonstration of (semi-)autonomous driving in the forest using these vehicles. Therefore, it necessitates the development of a nonlinear simulation platform to test, for example, navigation and control methods for these vehicles. This study focuses on the tire lateral forces in vehicle handling simulations.

The *magic formula* illustrated in Pacejka (2012) has been used for almost 30 years to model the lateral tire forces. It is magic as it suggests an empirical tire model and does not depend on first principles for its derivation. Naturally, it requires extensive testing to estimate several coefficients used in the formula. The magic formula, however, depicts that the relation between the tire's lateral force F_y and the sideslip angle α is linear at the origin (of the F_y versus α curve). Pacejka (2012) further illustrates that at $\alpha = 0$, the slope of the F_y versus α curve – defined as the cornering stiffness C_α – is not considerably influenced by the variations in speed and driving conditions.

Dixon (1988) noted four types of handling regions for a ground vehicle (either car or truck) by describing the variation of the steering angle δ_s with the lateral acceleration a_c. The range of a_c in the primary handling regime goes up to 3 m/s^2 for cars and 1 m/s^2 for trucks. For this range of a_c, the steering angle δ_u required in addition to the Ackermann steering angle δ_A is directly proportional to the lateral acceleration, where the constant of proportionality is the understeer gradient K_u. Therefore, if we restrict the scope of vehicle handling to the primary handling regime, a linear tire behavior depicting the relationship between F_y and α would be adequate (see, for example, Pauwelussen (2014)).

The cornering stiffness value of a tire primarily depends on the constructions of its carcass (Wong (2008)). A tire's carcass consists of several rubber-coated plies (cords). The geometrical layout of these plies on top of one another determines the characteristics of a tire and the vehicle dynamics in the primary handling regime, that is when $a_c < 3$ m/s^2 for cars (Dixon (1996)). Bias-ply tires (also known as cross-ply tires) have a low angle of about 40° between the circumferential centerline of the tire and the plies. This angle is known as the crown angle (Wong (2008); Dixon (1996)). Radial-ply tires have one or more plies at a 90° crown angle. A low crown angle depicts better cornering properties, whereas a tire with a high crown angle has better ride comfort (Wong (2008)).

Wong (2008) notices that the lateral force F_y of a bias-ply tire increases slowly with an increase in α than that of a radial-ply tire. The two main factors that affect the cornering properties of a tire include the vertical load and the inflation pressure. The impact of varying inflation pressure over the cornering is small, especially for the bias-ply tires. However, the load significantly

⋆ The research is funded by the Technology Industries of Finland Centennial Foundation and Jane and Aatos Erkko Foundation.

10.1016/j.ifacol.2022.11.107

influences the lateral force generated by a tire. A parameter called cornering (stiffness) coefficient C_{C_α} often describes the effect of load on cornering. Dixon (1996) mentioned (1) linear, (2) power, and (3) exponential models to describe the variation of cornering (or lateral force) coefficients with the load. In general, the cornering coefficients for bias-ply tires at rated load is lower than the radial-ply tires; see, as an example, (Wong, 2008, Table. 1.4). Moreover, the rise of the cornering stiffness values for light and heavy truck tires stay almost linear beyond the rated load; see, for example, (Wong, 2008, Fig. 1.27).

To find an initial estimate of the cornering stiffness is the first and foremost step in modeling lateral forces in vehicle handling simulation. However, the only practical way to determine C_α is through experiments, which are expensive and time-consuming (see, for example, Georgieva and Kunchev (2015); Vorotović et al. (2013)). To circumvent such extensive experimentation, Hewson (2005) derives an expression for the cornering stiffness of the tire in terms of the basic tire parameters. Hewson's model, too, considers a linear region of the vehicle handling domain. Although Hewson's study concerns radial-ply tires, the same can be true for a bias-ply tire. Since the only factor in the expression of C_α estimated from the tire data is the modulus of elasticity (E) of the beam structure. This quantity is associated with the lateral displacement (hence, the lateral stiffness) of the tire's belt in the beam model. It is noteworthy that the lateral stiffness for heavy truck tires, either with a radial-ply or a bias-ply construction, does not vary much, as illustrated in (Wong, 2008, Section 1.4.4).

The organization of the rest of the document is as follows. Brief details about the 6-DOF (6 degrees of freedom) model of the vehicle used in the simulation is provided in Section 2. It follows by describing the tire lateral force equations used in the simulations. The determination of cornering coefficients of tires used in Polaris and Bison is carried out in Section 3. Simulation results are presented in Section 4. Lastly, critical observations from this study are highlighted in the conclusions section.

2. VEHICLE MODEL

A higher-order model is necessary to, for example, include the dynamics of suspension heights installed at each corner of the car. However, the inclusion of these additional dynamics always comes at a price of higher computational frequency to capture the comprehensive dynamics of the system. The reason is the model of a tire, if included as the mass-spring system to the simulation, introduces high frequencies. For bias-ply tires, it is an issue as the vertical stiffness of such tires is very high (see, for example, the discussion about Ride Comfort in Wong (2008)). Since the natural frequency of the mass-spring system is inversely proportional to the coefficient of stiffness of the spring, the corresponding frequency of the tire would be very high compared to the sprung mass. Thus, we restrict ourselves to a 6-DOF model corresponding to the sprung mass of the vehicles instead of an exhaustive 14-DOF model (as illustrated in Shim and Ghike (2007)) to design a simulation that runs at a reasonably lower computational frequency. Thus, in this study, the tire only introduces a central force component (F_s) and a drag force component (F_d) to the 6-DOF model via the steering angle (Dixon (1996)).

2.1 Nonlinear 6-DOF vehicle model

The vehicle is considered as a rigid body with a frame (xyz) fixed to its center of gravity (CG). The position coordinates (X, Y, Z) represent the position of vehicle's CG in a 3D inertial (fixed) frame of reference. The body frame velocities, i.e. the linear velocities of the vehicle CG are defined as longitudinal (forward) velocity (u), lateral (left-side) velocity (v), and up velocity (w). The state vector contains roll rate (p), pitch rate (q), and yaw rate (r) which are the angular velocities of the vehicle frame. Finally, the state vector constitutes Euler angles roll angle (ϕ), pitch angle, and yaw angle. Thus, the state vector is defined as $\mathbf{X} = \{X, Y, Z, u, v, w, p, q, r, \psi, \theta, \phi\}$ with the equations of motions collected from Shim and Ghike (2007); Etkin and Reid (1995) are as follows:

$$\begin{aligned}\dot{X} &= u\cos\theta\cos\psi + v(\cos\psi\sin\theta\sin\phi - \cos\phi\sin\psi) \\ &\quad + w(\sin\phi\sin\psi + \cos\phi\cos\psi\sin\theta)\end{aligned} \tag{1}$$

$$\begin{aligned}\dot{Y} &= u\cos\theta\sin\psi + v(\cos\phi\cos\psi + \sin\theta\sin\phi\sin\psi) \\ &\quad + w(\cos\phi\sin\theta\sin\psi - \cos\psi\sin\phi)\end{aligned} \tag{2}$$

$$\dot{Z} = -u\sin\theta + v\cos\theta\sin\phi + w\cos\theta\cos\phi \tag{3}$$

$$\dot{u} = \frac{\mathbf{F}_x}{m} + g\sin\theta - qw + rv, \tag{4}$$

$$\dot{v} = \frac{\mathbf{F}_y}{m} - g\sin\phi\cos\theta + pw - ru, \tag{5}$$

$$\dot{w} = \frac{\mathbf{F}_z}{m} - g\cos\phi\cos\theta - pv + qu, \tag{6}$$

$$\dot{p} = \frac{\mathbf{L} - qr(I_{zz} - I_{yy})}{I_{xx}}, \tag{7}$$

$$\dot{q} = \frac{\mathbf{M} - rp(I_{xx} - I_{zz})}{I_{yy}}, \tag{8}$$

$$\dot{r} = \frac{\mathbf{N} - pq(I_{yy} - I_{xx})}{I_{zz}}, \tag{9}$$

$$\dot{\psi} = \frac{q\sin\phi + r\cos\phi}{\cos\theta}, \tag{10}$$

$$\dot{\theta} = q\cos\phi - r\sin\phi, \tag{11}$$

$$\dot{\phi} = \dot{\psi}\sin\theta + p. \tag{12}$$

In above equations, $\mathbf{F}_x$, $\mathbf{F}_y$, and $\mathbf{F}_z$ are forces experienced by the vehicle body along x, y, and z axes, respectively. m is the sprung mass of the vehicle. I_{xx}, I_{yy}, and I_{zz} are the moments of inertia of the rigid body around its CG. $\mathbf{L}$, $\mathbf{M}$, and $\mathbf{N}$ are the rolling, pitching and yawing moments of the vehicle body, respectively. The forces and moments include those transmitted to the sprung mass via suspensions – modeled as spring-damper systems – at each corner of the vehicle (Shim and Ghike (2007)).

2.2 Tire Lateral forces

In the coordinate frame $(x'y'z')$ fixed to center of each wheel, the lateral slip angle is given as (Shim and Ghike (2007))

$$\alpha_{kl} = \tan^{-1}\left(\frac{v_{g_{kl}}}{u_{g_{kl}}}\right) - \delta_{A,kl}, \tag{13}$$

where, the subscript (kl) represents left front (lF), right front (rF), left rear (lR), and right rear (rR) tires. $\delta_{A,kl}$ denotes the Ackermann's steering angle, where for rear ones $\delta_{A,kR} = 0$. $u_{g_{kl}}$, $v_{g_{kl}}$, and $w_{g_{kl}}$ are the longitudinal, lateral, and vertical velocities at the tire contact patch, respectively. These velocities can be obtained by transforming the CG velocities (see, for example, Shim and Ghike (2007)).

In the primary handling regime, the lateral tire force is related to the sideslip angle as

$$F_{y_{t_{kl}}} = -C_{\alpha,kl}\alpha_{kl}, \tag{14}$$

where $C_{\alpha,kl}$ is the cornering stiffness of klth tire. The subscript t represents the forces in the wheel fixed coordinate frame. Here, we consider a linear relationship between cornering stiffness and vertical force (Vorotović et al. (2013)), given as

$$C_{C_{\alpha,kl}} = \frac{C_{\alpha,kl}}{F_{z_{t_{kl,0}}}}, \tag{15}$$

where $C_{C_{\alpha,kl}}$ is the cornering stiffness coefficient, and $F_{z_{t_{kl,0}}}$ is the normal force on the klth tire at its maximum rated load and the given inflation pressure. This, ultimately leads to the following relationship between the lateral force and the vertical force on each tire

$$F_{y_{t_{kl}}} = -C_{C_{\alpha,kl}} F_{z_{t_{kl}}}\alpha_{kl}. \tag{16}$$

The longitudinal force on the klth tire is computed as

$$F_{x_{t_{kl}}} = \mu F_{z_{t_{kl}}}, \tag{17}$$

where μ is the rolling resistance coefficient (Dixon (1996)). These wheel forces in body frame are obtained by transforming the tire aligned forces to the strut (vehicle motion) aligned forces. Such transformation is obtained by (Shim and Ghike (2007))

$$\begin{bmatrix} F_{x_{b_{kl}}} \\ F_{y_{b_{kl}}} \\ F_{z_{b_{kl}}} \end{bmatrix} = \mathbf{R}_x(-\phi)\mathbf{R}_y(-\theta)\mathbf{R}_z(\delta_{kl}) \begin{bmatrix} F_{x_{t_{kl}}} \\ F_{y_{t_{kl}}} \\ F_{z_{t_{kl}}} \end{bmatrix}, \tag{18}$$

where $\mathbf{R}_x(\cdot)$, $\mathbf{R}_y(\cdot)$, and $\mathbf{R}_z(\cdot)$ are the rotation matrices about x, y, and z axes, respectively (see, for example, Etkin and Reid (1995) for the definition of rotation matrices). The subscript b represents the forces in the vehicle body frame.

3. ESTIMATION OF C_α

Both machines use bias-ply tires as their objective is to transport heavy loads at low speeds on uneven terrains. Bison forwarder is by default an 8-wheeler articulated machine that uses Nokian Forestry F2 tires with sidewall ratings 710/45-26.5, whereas Polaris e-ATV comprises of 4 Carlisle's 25×9.00-12 tires. The important parameters for both tires are highlighted in Table 1.

Table 1. Tire Parameters

Quantity	Bison	Polaris	Unit
Manufacturer	Nokian	Carlisle	–
Rating	710/45-26.5	25×9.00-12	–
Radius (ρ)	336.55	152.4	mm
Thickness (τ)	35	19	mm
Width (ν)	710	228.6	mm
Aspect Ratio (a)	0.45	0.7	–
Sidewall Deflection (s)	0.1533	0.1	per unit
Ply Rating (PR)	20	4	–
Rated Load	6900	374.2	kg

In Hewson (2005), the expression of the cornering stiffness using basic tire parameters is given as

$$C_\alpha = \frac{2E\tau\nu^3}{(\rho+\nu a)^2 \sin(A)\,(\pi - \sin(A))}, \tag{19}$$

where ν is the belt width, τ is the belt thickness, ρ is the wheel radius, a is the wheel aspect ratio, s is the unitized (per cent) vertical deflection of the sidewall when loaded, and

$$A = \cos^{-1}\left(\frac{\rho+\nu a - s\nu a}{\rho+\nu a}\right).$$

The suggested values for parameters s and τ for road tires are 0.15 and 15 mm, respectively. Parameter τ is associated with the material thickness of the belt. Typically, a belt is the constituent parts of a radial-ply tire. However, the carcass of a bias-ply tire does not include belts. Besides, Hewson (2005) estimated the value of E from experimental data of a sample of radial-ply tires. Therefore, it again leads to the dependency of using experimental data to compute C_α. Here, we introduce a different approach to estimate s, τ, and E for the bias-ply tires.

Firstly, we select τ as the depth of the tread, which is usually mentioned in the tire datasheet. Thus, the belt thickness for the radial-ply tires is replaced with the tread thickness for bias-ply tires. Secondly, the computation of parameter s is as follows:

(1) Read the unloaded tire radius from the datasheet. We denote this quantity by

$$\rho_u = \rho + \nu a. \tag{20}$$

(2) Read the static loaded radius of the tire at the rated load and rated inflation pressure. This quantity becomes

$$\rho_i = \rho + \nu a - s\nu a. \tag{21}$$

(3) Calculate the value of s by using

$$s = \frac{\rho_i - \rho_u}{\nu a}. \tag{22}$$

As an example, we know $\rho_i = 670$ mm and $\rho_u = 622$ mm from the datasheet of Nokian Forestry F2 tires. The values of ρ, a, and ν are already provided in Table 1. Using Equation (22), we get $s = 0.1533$. This value of s matches closely to that suggested in Hewson (2005) for the road tires.

Lastly, we apply the concept of *friction ellipses* (see, for example, Wong (2008)) illustrated by

$$\left(\frac{F_y}{F_{y,max}}\right)^2 + \left(\frac{F_x}{F_{x,max}}\right)^2 \leq 1 \tag{23}$$

to select the value of E in the simulations. To achieve this, we specify the limits on longitudinal acceleration command a_{xc} and the curvature command K_c for the vehicle. In other words, a nominal speed command V_c is fixed such that the vehicle (car or truck) operates in the primary handling regime for the given K_c. Thus, for the given road conditions, assuming zero skidding, we select a value of E such that the simulated lateral force $F_y = F_y(\alpha, F_z, E)$ satisfies Equation (23). We will discuss the selection of E in the forthcoming section.

4. SIMULATION RESULTS

The important vehicle parameters are mentioned in Table 2. Notice that the Bison forwarder uses articulated steering mech-

Table 2. Vehicle Parameters

Quantity	Bison	Polaris	Unit
Type	Forwarder	e-ATV	–
Mass (Self)	22600	793.8	kg
Load Capacity	16000	455	kg
Length	10.3	2.74	m
Width	2.6	1.44	m
Height	3.9	1.85	m
Turning Radius	10	3.81	m
Nominal Speed	2	5	m/s
Max. Curvature	0.1	0.2625	m^{-1}

anism (see, for example, Li et al. (2013)), whereas Polaris e-ATV utilizes Ackermann's steering. For simulations, we model the dynamics of both type of vehicles as provided in Section 2.1 as the focus is on modeling lateral forces. The nominal speed mentioned in Table 2 is not the maximum rated speed of the vehicle rather it is the speed at which the vehicle nominally operates. For Bison, if we set $E < 5$ MPa, Equation (23)

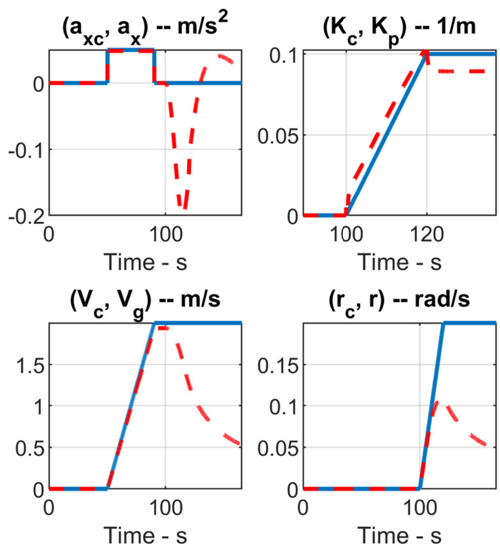

Fig. 1. The inputs forward acceleration command a_{xc}, speed command V_c, curvature command K_c, and yaw rate command r_c are shown in blue. The output responses of Bison (a_x, V_g, K_p, and r) are shown in (dashed) red. A zoomed-in (K_c, K_p) plot highlights oversteer.

is satisfied on flat terrain. At $E = 2$ MPa, $C_\alpha = 111,160$ N/rad for the Nokian 710/45-26.5 tire. The estimated value of $C_{C_\alpha} = 1.6439$ rad^{-1} at the rated load of 6900 kg.

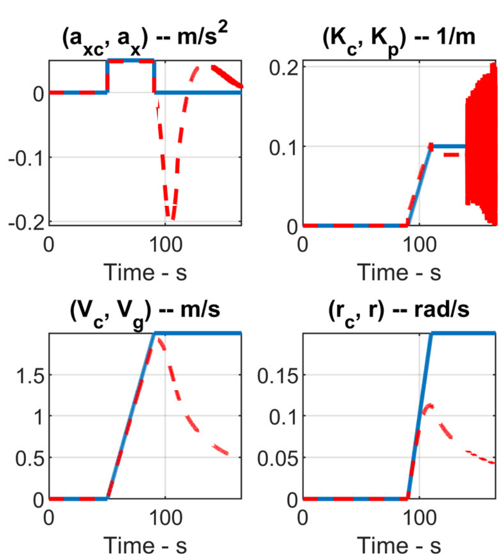

Fig. 2. The open loop response at $E = 5$ MPa. K_p is already oscillating at the end.

Figure 1 illustrates the open loop responses corresponding to forward acceleration $a_x = \dot{u}$, ground speed $V_g = \sqrt{u^2 + v^2}$, path curvature K_p, and yaw rate r of Bison forwarder at the above-mentioned values of E, C_α, and C_{C_α}. Here, the actual inputs to the dynamic model are the acceleration a_{xc} and curvature K_c commands. The speed command V_c is obtained by integrating a_{xc} while the commanded yaw rate r_c is illustrated by the product $K_c V_c$.

Figure 2 shows the open loop response of Bison forwarder when $E = 5$ MPa was selected. The vehicle curvature K_p starts oscillating when commanded curvature K_c is at the designated maximum value of 0.1 m^{-1} for the given speed command.

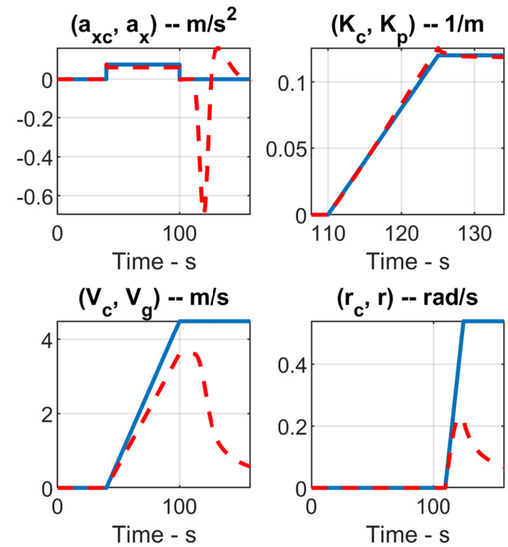

Fig. 3. Open loop forward acceleration a_x, ground velocity V_g, curvature K_p, and yaw rate r responses of Polaris when $E = 2$ MPa is selected.

In case of Polaris, unstable turns are obtained for $E > 2.25$ MPa on even terrain. At $E = 2$ MPa, the value of $C_\alpha = 10,419$ N/rad for the Carlisle 25×9.00-12 tire is obtained, which leads to a value of $C_{C_\alpha} = 2.8413$ rad^{-1} at the rated load of 374.2 kg. Figure 3 illustrates the open loop responses of Polaris e-ATV to the a_{xc} and K_c commands.

Hence, we can use $E = 2$ MPa for both vehicles to simulate lateral tire forces in the nonlinear 6-DOF simulation. It is crucial to highlight here that this value of E is well-matched to the average lateral stiffness value $k_d = 2.2275$ MPa provided in (Wong, 2008, Section 1.1.4) for heavy-duty truck tires.

5. DISCUSSIONS

It is important to mention here that for the selected nominal speed V_c, curvature command K_c for both vehicles is adjusted such that the condition $a_c < 1$ m/s^2 for Bison and $a_c < 3$ m/s^2 for Polaris is always satisfied. The value of $1/K_{c,max}$ (minimum turning radius) is usually provided in the datasheet of the vehicle. However, K_c is further tuned in the simulations to not compromise the nominal speed of the vehicle. As shown in Figure 3, the applied curvature command K_c for Polaris is limited to 0.15 m^{-1} – that is reduced from rated maximum of 0.2625 m^{-1} – when the commanded speed V_c is 4.5 m/s. These values of V_c and K_c corresponds to the lateral acceleration of about 3 m/s^2.

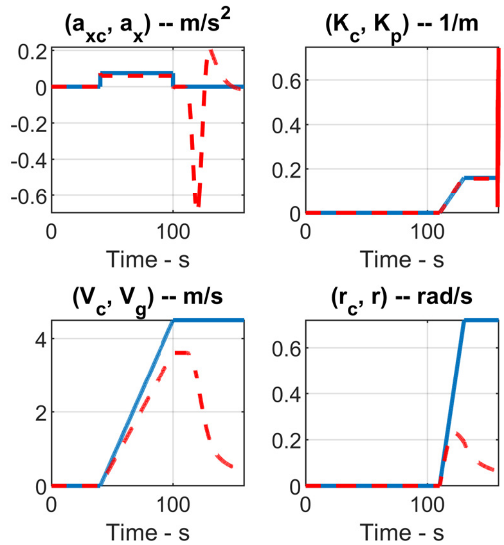

Fig. 4. Open loop state responses of Polaris when the condition $a_c < 3$ m/s^2 is violated. Notice the oscillations in K_p at the end of simulation.

On the other hand, Figure 4 shows simulation results highlighting an unstable case when the condition $a_c < 3$ m/s^2 is not satisfied for Polaris. In this case, the K_c at the end increases up to 0.16 m^{-1} given the same $V_c = 4.5$ m/s, which corresponds to $a_c = 3.2$ m/s^2. Therefore, special attention to lateral acceleration limits is required while utilizing Equation (16) to simulate lateral tire forces and Equation (19) to estimate C_α in the nonlinear ground vehicles simulation.

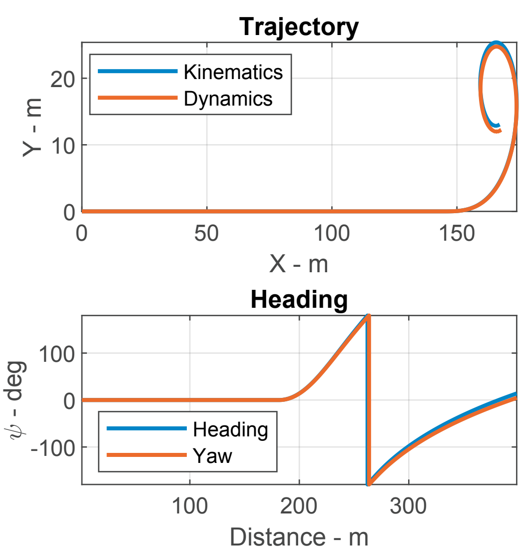

Fig. 5. (X, Y)-path and yaw (or heading) angle ψ results for Polaris e-ATV using dynamic model (shown in red) and kinematic model (shown in blue). Notice the similarity between graphs when the speed profile for both models are same.

In addition, two critical observations in the dynamic model simulation results are worth focusing on concerning the application of the lateral tire forces. These observations are made in comparison to those obtained from a standard kinematic model that excludes tire forces (we refer to Kelly (2013) for details about ground robot kinematics). First, there is a reduction in speed while the vehicle starts turning. From Equation (18), it is straightforward to write the vehicle motion aligned forces in terms of the wheel aligned force as

$$F_{x_{b_{kl}}} = F_{x_{t_{kl}}} \cos\delta_{kl} - \underbrace{F_{y_{t_{kl}}} \sin\delta_{kl}}_{F_d}, \tag{24a}$$

$$F_{y_{b_{kl}}} = F_{x_{t_{kl}}} \sin\delta_{kl} + \underbrace{F_{y_{t_{kl}}} \cos\delta_{kl}}_{F_s}. \tag{24b}$$

Thus, the tire lateral force $F_{y_{t_{kl}}}$ resolves into two components in the vehicle motion aligned forces $F_{x_{b_{kl}}}$ and $F_{y_{b_{kl}}}$ namely (1) drag force component F_d, and (2) central force component F_s. It is F_s that is providing necessary centripetal acceleration for the vehicle to turn in a circular path, whereas F_d is responsible for the deceleration of the vehicle (Dixon (1996)). Figure 5 highlights a similar observation noted in Karkee and Steward (2010) that the open loop responses of a high-fidelity dynamic model and a kinematic model match at operating velocities of about 0 to 4.5 m/s.

The second effect is the positive understeer gradient which is prominent in the simulations of both Bison forwarder and Polaris e-ATV. For the linear tire behaviour, the understeer gradient (Pauwelussen (2014))

$$K_u = \alpha_{kF} - \alpha_{kL}. \tag{25}$$

This positive understeer, often termed as the oversteer, produces a nonlinear yaw angle during the cornering of the vehicle which is depicted in Figure 5. Such nonlinear yaw is natural as the CG position is changing with the acceleration and deceleration of the vehicle. This shift induces a change in slip angles of the front and rear wheels. Since our model has nonlinear slip angles that are using wheel speed components $(u_{g_{kl}}, v_{g_{kl}})$ and Ackermann steering angle $\delta_{A,kl}$, oversteering occurs by means of the difference $\alpha_{kF} - \alpha_{kL}$. For Polaris, this effect is highlighted in Figure 3, where the resulting path curvature K_p starts leading the curvature command K_c at time 120 seconds.

6. CONCLUSIONS AND FUTURE WORK

This paper highlights the efficacy of using a linear tire model to simulate lateral tire forces, provided the vehicle handling is limited to the primary handling regime. At first, it is necessary to compute the cornering stiffness of a tire, which requires extensive testing on the tire. However, Hewson's model was effectively used to calculate the cornering stiffness value of two different bias-ply tires by using nothing but the tire datasheet specifications. The resulting lateral tire forces truly emulate vehicle deceleration during the turn. Moreover, the analysis of the simulation results illustrated the presence of the understeer gradient while the vehicle turns.

Only through repeated tests and evaluation on actual machines the utility of this study can be determined. However, this study is crucial in, for example, designing test scenarios for the ground vehicles. There is a need for a test procedure that capture realistic cornering behavior by fixing, for example, driving speed and steering angle. Once validated by real-time data, the simulation platform will provide a functional basis for furthering the mathematical model for forest machines considering uneven terrains.

ACKNOWLEDGEMENTS

The authors acknowledge the role of the Department of Electrical Engineering and Automation at Aalto University to make this research possible. Special thanks to the Technology Industries of Finland Centennial Foundation and Jane and Aatos Erkko Foundation for providing necessary funding for the AUTOLOGGER project under The Future Makers program.

REFERENCES

Dixon, J.C. (1988). Linear and non-linear steady state vehicle handling. *Proceedings of the Institution of Mechanical Engineers, Part D: Transport Engineering*, 202(3), 173–186.

Dixon, J.C. (1996). *Tires, Suspension and Handling*. SAE International, USA, second edition.

Etkin, B. and Reid, L.D. (1995). *Dynamics of Flight: Stability and Control*. John Wiley and Sons, USA, third edition.

Georgieva, H. and Kunchev, L. (2015). Experimental determination of tyre lateral force: Application to tyre cornering stiffness. *Applied Mechanics and Materials*, 798, 41–47.

Hewson, P. (2005). Method for estimating tyre cornering stiffness from basic tyre information. *Proceedings of the Institution of Mechanical Engineers, Part D: Journal of Automobile Engineering*, 219(12), 1407–1412.

Karkee, M. and Steward, B. (2010). Study of the open and closed loop characteristics of a tractor and a single axle towed implement system. *Journal of Terramechanics*, 47.

Kelly, A. (2013). *Mobile Robotics: Mathematics, Models, and Methods*. Cambridge University Press, Cambridge.

Li, X., Wang, G., Yao, Z., and Qu, J. (2013). Dynamic model and validation of an articulated steering wheel loader on slopes and over obstacles. *Vehicle System Dynamics*, 51(9), 1305–1323.

Pacejka, H.B. (2012). Chapter 1 - Tire Characteristics and Vehicle Handling and Stability. In *Tire and Vehicle Dynamics*, 1–58. Butterworth-Heinemann, Oxford, third edition.

Pauwelussen, J. (2014). Chapter 5 - Vehicle Handling Performance. In *Essentials of Vehicle Dynamics*, 123–194. Butterworth-Heinemann, Oxford, first edition.

Shim, T. and Ghike, C. (2007). Understanding the limitations of different vehicle models for roll dynamics studies. *Vehicle System Dynamics*, 45(3), 191–216.

Vorotović, G., Rakicevic, B., Mitić, S., and Stamenković, D. (2013). Determination of cornering stiffness through integration of a mathematical model and real vehicle exploitation parameters. *FME Transactions*, 41, 66–71.

Wong, J.Y. (2008). *Theory of Ground Vehicles*. John Wiley and Sons, Inc., New York, USA, fourth edition.